Available online at www.eccomasproceedia.org
Eccomas Proceedia UNCECOMP (2023) 284-296

ECCOMAS
Proceedia

UNCECOMP 2023
5th ECCOMAS Thematic Conference on
Uncertainty Quantification in Computational Science and Engineering
M. Papadrakakis, V. Papadopoulos, G. Stefanou (eds.)
Athens, Greece, 12-14 June 2023

MULTI-FIDELITY GAUSSIAN PROCESS SURROGATE MODELING FOR FLOW THROUGH STENOSIS

Shaima Magdaline Dsouza[1,2], Saleh Rezaeiravesh[3], Philipp Schlatter[1,4], Lisa Prahl Wittberg[1], T. Christian Gasser[2,5]

[1] FLOW, Department of Engineering Mechanics, KTH Royal Institute of Technology, Stockholm, Sweden. e-mail: (smdsouza, pschlatt, prahl, gasser)@kth.se

[2] Solid Mechanics, Department of Engineering Mechanics, KTH Royal Institute of Technology, Stockholm, Sweden.

[3] Department of Fluids and Environment, The University of Manchester, Manchester, UK, e-mail: saleh.rezaeiravesh@manchester.ac.uk

[4] Institute of Fluid Mechanics (LSTM), Friedrich–Alexander Universität Erlangen–Nürnberg, Germany.

[5] Faculty of Health Sciences, University of Southern Denmark, Odense, Denmark.

Abstract. *The blood flow characteristics found in our larger vessels are unsteady, particularly around the heart valves and bifurcations. In the case of stenosis, or narrowing of the vessels, the flow may transition to turbulence. To understand the dynamics of the forces acting on the blood components and the vessel wall, simulations using computational fluid dynamics (CFD) are commonly applied. The severity of the stenosis can be determined by accurately assessing the fluid flow, which can also serve as a risk indicator for potential thromboembolic events. Motivated by the vessel's geometry being a factor that highly influences the flow characteristics, we investigate here the impact of changes in geometry on turbulence using multi-fidelity models, which are based on Gaussian processes. The objective is to develop a multi-fidelity model to construct a high-fidelity estimate by combining numerical simulations from spectral element-based direct numerical simulations (DNS) and finite volume-based Reynolds-Averaged Navier-Stokes (RANS) simulations. Specifically, a co-kriging-based model with Gaussian process is used to combine various levels of fidelity (RANS, DNS). To vary the blood vessel geometry, the stenosis's severity and eccentricity are considered uncertain input parameters. A multi-fidelity model is then used to predict the consequences of said uncertainties on the mean pressure drop across the vessel and the wall shear stress, the quantities of interest directly linked to the biological activity of the vessel. Using data of different accuracy, the multi-fidelity technique allows us to optimize the accuracy and cost of predictions.*

Keywords: Multi-fidelity models, Gaussian processes, Uncertainty quantification, Stenosis, Turbulence.

ISSN:2623-3339
Peer-review under responsibility of the organizing committee of UNCECOMP 2023.
doi: 10.7712/120223.10338.19836

1 INTRODUCTION

According to World Health Organization (WHO), cardiovascular diseases (CVD) are one of the most common causes of death worldwide[1]. An abnormal narrowing of human arterial vessels, known as stenosis, is often caused by a local plaque buildup. In the case of plaque rupture, there is an increased risk of downstream blockage that may result in stroke, a leading cause of death and disability [1]. Consequently, there has been, and still is, extensive research focused on understanding plaque initiation and buildup to predict and identify risk potential and improve treatment efficiency. From an engineering perspective, detailed flow analysis has gained increasing attention with the increased available computational power. This has allowed us to understand the disease dynamics better and estimate its contributing factors. However, measuring wall shear stress (WSS) and hemodynamic parameters in vivo remains a challenge [2]. Despite being an attractive alternative, simulating with a variation of multiple parameters incurs a high computational cost. Moreover, the input parameters for these models are never precisely known due to patient-specific conditions and measurement noise [3]. Also, there is a lack of knowledge and models to determine the payoff of risk versus complications of the operation itself [4]. Therefore, considering and quantifying the uncertainties arising from the patient-specific analysis is essential to improve our understanding of CVDs.

The Monte Carlo (MC) method is commonly used for uncertainty propagation. MC necessitates many input random variable samples to calculate the output variables repeatedly. A large number of samples are required for accurate estimates. However, the computational cost can be a significant obstacle [5]. To overcome this barrier, surrogate models have been designed, also known as metamodels, proxy models, model emulators, or response surfaces [6]. These models approximate the primary features of the complex model in the space of inputs or parameters, resulting in an improved accuracy versus cost trade-off. While providing inexpensive approximations using sparse data, these models may need to represent the quantities of interest (QoIs) accurately. Furthermore, obtaining a surrogate model to a complex model may still requires unaffordable computational cost, mainly when dealing with a large number of parameters (the curse of dimensionality) [7].

Gaussian processes (GP) [8] are widely used for regression, classification, and prediction due to their flexibility in modeling relationships between a model's input and outputs. Initially developed in geostatistics by Daniel Krige as the "kriging" model to predict ore grades from spatially correlated sample data in South African gold mines, it was later formalized by Matheron [9]. Since then, GP models have gained popularity in various fields, including finance, healthcare, marketing, computer vision, and robotics. GP models are beneficial for problems requiring interpolation and extrapolating of limited and noisy data, providing probabilistic estimates of the prediction error. In terms of prediction accuracy, GP models have been shown to outperform other popular models, such as adaptive regression splines, support vector machines, and neural networks [10].

The multivariate extension of kriging is called co-kriging [11]. Co-kriging employs a sparsely sampled target variable compared to a densely sampled auxiliary variable. The spatial correlation between the target and auxiliary variables is modeled using a covariance function. This allows for estimating the target variable at unobserved locations based on the observed values of related variables. Thus co-kriging enables the fusion of the variable fidelity (high and low) data to develop predictive models. The idea of incorporating information from simulations at different levels of fidelity is useful when the simulations at a higher level of fidelity are more

[1] https://www.who.int/health-topics/cardiovascular-diseasestab=tab$_1$

expensive but, at the same time, significantly more accurate than simulations at a lower fidelity level. The higher-fidelity simulations can be used to model the correlation between the target variable and related variables. The co-kriging method was extended by [12] using the GPs for multi-fidelity regression. The multi-fidelity regression method has been further improved to include several levels of fidelities to handle large data sets [13], and made computationally more efficient by applying a recursive algorithms [14]. A predictive model that calibrates each computer model to the next fidelity level and then calibrates the highest fidelity simulator to field measurements was proposed by [15]. The latter employs the Gaussian process to represent all fidelities and corrections and a Bayesian hierarchical model to combine different sources of information for predictions. This model has been adapted and applied to turbulent flow problems in Ref. [16]. A class of Bayesian neural networks was developed by [17]. They trained the model using variable fidelity noisy data to learn function approximations and resolve inverse problems based on partial differential equations.

There is a need to improve the understanding of problems in the analysis of hemodynamics. The evaluation of flow responses from the Navier-Stokes equations can be computationally expensive. Developing optimization methods requiring the fewest number of data samples has been of utmost importance [18]. Recently, there has been an increased interest in enhancing the predictions from the Reynolds Averaged Navier-Stokes (RANS) models. They play a significant role in ensuring engineering designs' reliability, safety, and efficacy. However, there are limitations to using the data available from the measurements in hemodynamics. Patient-specific data, for instance, can be difficult, expensive, or even impossible to get, and ethical concerns might limit the amount of data provided [19]. Therefore, it is desirable to have the fusion of data from different fidelity levels of computer simulation, which will provide a more accurate characterization of the disease and facilitate improved planning and delivery of the treatment. The literature on multi-fidelity methods in haemodynamics remains limited. Only a handful of studies have explored the application of multi-fidelity in haemodynamics research, making it an area ripe for further investigation. The estimation of hemodynamics parameters using model inversion that employs GP and Bayesian optimization [20], multilevel multi-fidelity (MLMF) Monte Carlo estimator method based on spatial complexity and varying spatial resolution [21]. Their approach has proved to be efficient for uncertainty propagation in large-scale hemodynamic problems. A fusion framework motivated by scalable supervised learning algorithms to explore cross-correlations between variable fidelity blood flow models was proposed in Ref. [20]. The high-dimensional optimized response surfaces are constructed while minimizing the number of expensive function evaluations. The framework was robust in the presence of model inaccurate low-fidelity models or noisy measurements.

A multi-fidelity approach between a 3D cardiac model and a simplified 0D version to speed up an efficient parameter estimation algorithm was proposed in Ref. [22]. This method leads to a fast and computationally efficient personalization method of the 3D model. A bi-fidelity Uncertainty Quantification (UQ) framework for 3D hemodynamic simulations was proposed based on a multi-fidelity stochastic collocation scheme in Ref. [23]. The low-fidelity model was used to inform the global searches over the parameter space and to help the high-fidelity reconstruction. The low-fidelity model assisted the high-fidelity reconstruction and global searches across the parameter space. Various cardiovascular flow cases, patient-specific artery geometries, and combinations of high- and low-fidelity models, such as 2D models and unconverged solutions, were used to assess the method's efficacy. A hybrid 3D and 1D model approach to determine the physiological condition of coronary lesions based on patients' specific data was presented in Ref. [24]. This hybrid model reduced the computational cost by approximately 1000 times.

In addition, the 1D reduced-order models naturally addressed the challenges associated with treating boundary conditions for 3D models.

In the present work, we investigate the mean pressure drop across the vessel and the wall shear stress (WSS) hemodynamic parameters most commonly reported as risk indicators in hemodynamic research. The data from Direct Numerical Simulations (DNS) and Reynold's Averaged Navier-Stokes (RANS) simulations are combined within a multi-fidelity framework [12]. Due to the conceptual differences between these models, correlation or correction coefficients are used to establish a connection and build a multi-fidelity model.

The remaining parts of the paper are organized as follows; Section 2 briefly overviews the GP and the multi-fidelity framework employed in this work. This section also presents numerical modeling parameters and briefly describes the DNS (high-fidelity) and RANS (low-fidelity) simulations. The results and discussions are presented in Section 3 followed by conclusions in Section 4.

2 METHODOLOGY

This section briefly overviews kriging (a Gaussian process) and co-kriging used for this work. The description of the numerical case is then presented.

2.1 Gaussian process

This section briefly discusses the Gaussian Process (GP); for a complete overview, readers are referred to Ref. [6, 8]. Consider a regression model for a quantity of interest y,

$$y = f(\mathbf{x}) + \epsilon, \tag{1}$$

where $\mathbf{x} = [x_1, x_2, \cdots, x_p]$ is the input vector, and $\boldsymbol{\epsilon}$ is the noise in the observed data that can be assumed as a white noise with zero-mean Gaussian distribution:

$$\boldsymbol{\epsilon} \sim \mathcal{N}(\mathbf{0}, \boldsymbol{\sigma^2}). \tag{2}$$

The function $f(\mathbf{x})$ in Equation (1) can be represented by a GP with a mean function $m(\mathbf{x})$ and covariance function $k(\mathbf{x}, \mathbf{x}^{'})$:

$$f(\mathbf{x}) \sim \mathcal{GP}(m(\mathbf{x}), k(\mathbf{x}, \mathbf{x}^{'})), \tag{3}$$

$$m(\mathbf{x}) = \mathbb{E}[f(\mathbf{x})], \tag{4}$$

$$k(\mathbf{x}, \mathbf{x}^{'}) = \mathbb{E}[(f(\mathbf{x}) - \boldsymbol{m}(\mathbf{x}))(f(\mathbf{x}^{'}) - \boldsymbol{m}(\mathbf{x}^{'}))], \tag{5}$$

For our case, we assume zero-mean Gaussian distribution. Therefore, $m(\mathbf{x}) = \mathbf{0}$. k in Equation (5) is the covariance kernel of the GP, the choice of which is based on the likely patterns and the smoothness of the underlying data in the space of the inputs. Gaussian (quadratic exponentiated), exponential, Matérn, periodic, and polynomial kernels are a few kernel functions that are widely used [8]. It is possible to combine different kernel functions by addition, multiplication, and convoluting to model complex functions. In the present work, we employ the Gaussian kernel known as the quadratic exponentiated kernel:

$$k(\mathbf{x}, \mathbf{x}^{'}) = \sigma_f^2 \exp\left(-\frac{||\mathbf{x} - \mathbf{x}^{'}||_2}{2\lambda^2}\right), \tag{6}$$

where λ (length scale) and σ_f^2 are the hyper-parameters optimized by maximizing the marginal likelihood given a set of data $(\mathbf{X}, \mathbf{Y})$. Once the Gaussian process is defined, the posterior function (at samples $\mathbf{X}^*$) is obtained that is conditioned upon the given observations as $p(\mathbf{Y}^*|\mathbf{X}^*, \mathbf{X}, \mathbf{Y})$. The estimation of the posterior function requires constructing a covariance function $\mathbf{K}^*$ between the data $\mathbf{X}$ and $\mathbf{X}^*$. The corresponding mean and the variance $m(\mathbf{Y}^*)$ and var($\mathbf{Y}^*$) at the test value $\mathbf{X}^*$ can be obtained as:

$$m(\mathbf{Y}^*) = \mathbf{K}^{*T}\mathbf{K}^{-1}\mathbf{Y}, \tag{7}$$

$$\text{var}(\mathbf{Y}^*) = \mathbf{K} - \mathbf{K}^{*T}\mathbf{K}^{-1}\mathbf{K}^*. \tag{8}$$

2.2 Co-kriging

Co-kriging surrogate modeling [25] can combine two data sets. Further improved results or outcomes can be obtained by incorporating more low-fidelity and fewer high-fidelity samples, an advantage when high-fidelity samples are either difficult to obtain or computationally costly. The observation vector for the co-kriging model $\mathbf{X}$ has both the observations from the low-fidelity $\mathbf{X}_{lf} = X_{lf_1}, X_{lf2}, \cdots, X_{lfNlf}$ and high-fidelity model $\mathbf{X}_{hf} = X_{hf1}, X_{hf2}, \cdots, X_{hfNhf}$, stacked together: $\mathbf{X} = [\mathbf{X}_{lf}; \mathbf{X}_{hf}]^T$, with the corresponding sample function values written as $\mathbf{Y} = [\mathbf{Y}_{lf}; \mathbf{Y}_{hf}]^T$. The GP model for two processes can be given as follows:

$$\boldsymbol{Z}_{hf} = \rho \boldsymbol{Z}_{lf} + \boldsymbol{Z}_d, \tag{9}$$

where ρ and $\boldsymbol{Z}_d$ are respectively the correlation coefficient and the difference between the high-fidelity $\boldsymbol{Z}_{hf}$ and low-fidelity models $\boldsymbol{Z}_{lf}$. The covariance for the kriging model in Equation (6) is employed to get the kernel for the co-kriging model [26]:

$$k(\mathbf{Y}_{lf}(\mathbf{X}_{lf}), \mathbf{Y}_{lf}(\mathbf{X}_{lf})) = k(\boldsymbol{Z}_{lf}(\mathbf{X}_{lf}), \boldsymbol{Z}_{lf}(\mathbf{X}_{lf})) = \boldsymbol{\Psi}_{lf}(\mathbf{X}_{lf}, \mathbf{X}_{lf}), \tag{10}$$

$$k(\mathbf{Y}_{hf}(\mathbf{X}_{hf}), \mathbf{Y}_{lf}(\mathbf{X}_{lf})) = k(\rho\boldsymbol{Z}_{lf}(\mathbf{X}_{hf}) + \boldsymbol{Z}_d(\mathbf{X}_{hf}), \boldsymbol{Z}_{lf}(\mathbf{X}_{lf})) = \rho\boldsymbol{\Psi}_{lf}(\mathbf{X}_{lf}, \mathbf{X}_{hf}), \tag{11}$$

$$\begin{aligned} k(\mathbf{Y}_{hf}(\mathbf{X}_{hf}), \mathbf{Y}_{hf}(\mathbf{X}_{hf})) &= k(\rho\boldsymbol{Z}_{lf}(\mathbf{X}_{hf}) + \boldsymbol{Z}_d(\mathbf{X}_{hf}), \rho\boldsymbol{Z}_{lf}(\mathbf{X}_{hf}) + \boldsymbol{Z}_d(\mathbf{X}_{hf})) \\ &= \rho^2\boldsymbol{\Psi}_{lf}(\mathbf{X}_{hf}, \mathbf{X}_{hf}) + \boldsymbol{\Psi}_d(\mathbf{X}_{hf}, \mathbf{X}_{hf}), \end{aligned} \tag{12}$$

The overall kernel matrix $\mathbf{K}_{CK}$ is given by:

$$\mathbf{K}_{CK} = \begin{bmatrix} \boldsymbol{\Psi}_{lf}(\mathbf{X}_{lf}, \mathbf{X}_{lf}) & \rho\boldsymbol{\Psi}_{lf}(\mathbf{X}_{lf}, \mathbf{X}_{hf}) \\ \rho\boldsymbol{\Psi}_{lf}(\mathbf{X}_{lf}, \mathbf{X}_{hf}) & \rho^2\boldsymbol{\Psi}_{lf}(\mathbf{X}_{hf}, \mathbf{X}_{hf}) + \boldsymbol{\Psi}_d(\mathbf{X}_{hf}, \mathbf{X}_{hf}) \end{bmatrix}. \tag{13}$$

The estimation of the mean and variance of the multi-fidelity model at $\mathbf{X}^*$ are similar to the kriging model; refer to Equation (7) and Equation (8), respectively. We employ the co-kriging framework available in GPy [2] in this work.

2.3 Numerical modeling and flow parameters

A vessel diameter D and length $19D$ were considered, with no-slip boundary conditions prescribed at the wall. Concentric and eccentric stenosis with the diameter D_s were investigated; see Figure 1. The severity of the stenosis is defined as the percentage reduction in the area:

$$SI = \frac{D^2 - D_s^2}{D^2} \times 100, \tag{14}$$

[2] https://github.com/SheffieldML/GPy

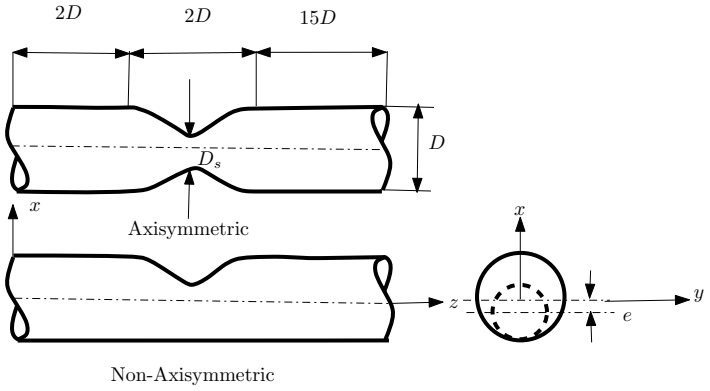

Figure 1: Schematic diagram showing axisymmetric and non-axisymmetric stenotic vessels.

The shape of the stenosis $S(z)$ is such that the cross-section of the vessel is a circle along the vessel [27]:

$$S(z) = \frac{D}{2}\left[1 - SI(1 - cos2\pi\frac{(z - z_0)}{L_s})\right], \tag{15}$$

where z_0 and L_s denote the onset and total length of the stenosis, respectively. The eccentricity in the stenosis geometry is given:

$$e(z) = E\frac{D}{2}\left[SI(1 - cos2\pi\frac{(z - z_0)}{L_s})\right]. \tag{16}$$

where E $\in [0, 100]$ (the values are in percentage), with e =0 specifying the stenotic vessel with no eccentricity.

The low-fidelity RANS simulations and high-fidelity DNS were performed at a Reynolds number (Re) of 2000, based on the bulk velocity through the vessel (U_b) and the vessel diameter (D). The parabolic velocity profile for laminar fully developed Poiseuille flow was imposed at the inlet. The Reynolds number was selected to encompass a wide range of turbulent scales to ensure both relevance of the low-fidelity RANS and manageable computational time for high-fidelity DNS. We assume blood to be a Newtonian fluid; this is a reasonable assumption for the rheological behavior of blood in the larger blood vessels [28]. The plaque is modeled as rigid (calcified) structures and only affected the fluid flow by constricting the flow channel (vessel lumen).

2.4 Details of DNS and RANS

The open-source Computational Fluid Dynamics (CFD) software Nek5000[3] was used in this study. The incompressible Navier-Stokes equations are discretized in space using a spectral element method using high-order Galerkin approximations with tensor-product polynomials bases. The polynomial order P_n-P_{n-2} was used to formulate the velocity and pressure curves. The bases in each grid element used for the DNS was made up of polynomial order $P_n = 9$ in each spatial direction, where there are $E = 4940$ hexahedral elements. The domain has about 3.6 million grid points [27].

The open-source code OpenFOAM[4] was used for the RANS simulations using the k-ω shear stress transport (SST) model [29]. This model has been used for blood flow in arteries and

[3]https://nek5000.mcs.anl.gov/
[4]https://www.openfoam.com/

veins, stenotic blood vessels, atherosclerosis (plaque buildup), aneurysms (ballooning of blood vessels), and heart valve flow simulations [30]. The k-ω SST model is often preferred for simulating these problems due to its ability to capture boundary layer and free-stream turbulence effects [30]. For RANS, the mesh consisted of C =1401820 hexahedral cells. The resolution was chosen after performing the convergence study on the residuals. The steady-state simulations were performed using the SimpleFOAM solver. The mesh resolution was such that the number of grid points in RANS and DNS were close to each other. Since, the main focus was to obtain a multi-fidelity model without extracting information from the different levels of mesh resolution.

3 RESULTS AND DISCUSSION

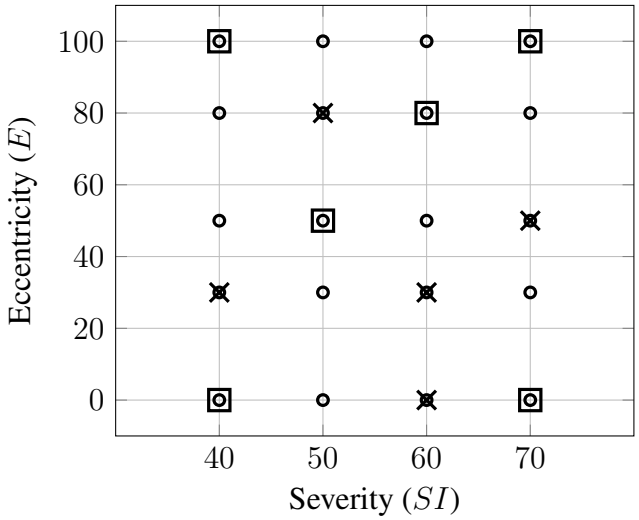

Figure 2: Schematic representation of the samples from SI and E corresponding to low-fidelity RANS (○), high-fidelity DNS (□), and validation set (DNS values are taken as truth) (×).

The stenosis test case as represented in Figure 1 was considered with two random input variables, i.e., variation in SI and variation in E. For the current study, we assumed a severity between 40% and 70% (refer to Equation (14)), a range within which medical decision-making is challenging. The stenosis geometry was chosen between the axisymmetric to non-axisymmetric by varying the parameter E in Equation (16). The stenosis severity significantly affects the WSS [31], and is known to be an atherosclerosis risk factor [32] because of the inflammatory response from the endothelial cells, causing the remodeling of the vessel. Thus, time-averaged WSS across the stenotic vessel and mean pressure drop across the stenotic vessel were investigated. Figure 2 illustrates the analyzed range of input variability and the data samples used for constructing the co-kriging multifidelty and kriging models.

The instantaneous coherent structures, isosurfaces of a negative contour of the λ_2 criterion for the case with maximum severity and fully eccentric vessel ((SI, E)=(70,100)), represents the nature of turbulent breakdown in the post-stenotic flowfield as shown in Figure 3. In the region close to the center of the stenosis in Figure 3, the vortices are observed that extend along the vessel length from $3D$ up to $13D$. These vortices are deemed essential in the flow transition from laminar to turbulent [27]. The quantities that are of intertest to assess the stenotic vessel are mean pressure drop and WSS.

The comparison of the mean pressure drop at the reference values from DNS GPR model,

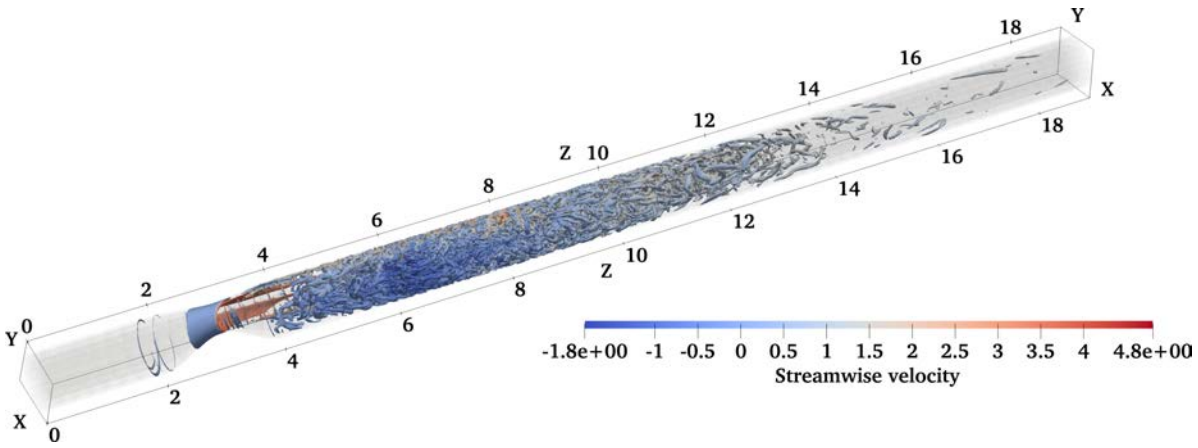

Figure 3: Instantaneous coherent structures (vortices) identified by using the isosurface corresponding to the 4.0 value of the λ_2 criterion for the case with SI=75% severity and fully eccentric $E = 100$ stenosis.

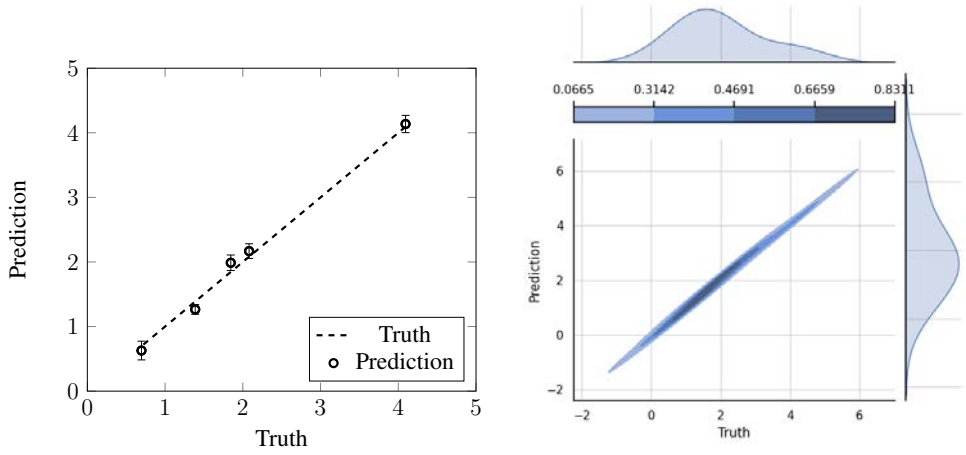

(a) (b)

Figure 4: (a) The truth versus prediction of the mean pressure drop across the stenotic vessel using the co-kriging model, (b) the joint PDF of the mean pressure drop.

and at the validation points ($\times$) are shown in Figure 4(a). For this case, we construct a kriging model (truth) by using the DNS available at ($\times$) and ($\square$). It can be observed that the predictions are close to the truth (dashed line); also, the $\pm 1.96\sigma$ (where σ is the standard deviation of the prediction) are shown as error bars in Figure 4(a) around the predicted values. This implies that the predictions are 95 % confident to lie within the range of the error bars in Figure 4(a). The joint and marginal Probability Density Function (PDF) of the truth and the predictions are found using the KDE (kernel density estimation) method and are shown in Figure 4(b). The marginal PDF of the predictions is close to the reference as observed from the Figure 4(b). The predictions of WSS from the multi-fidelity model are compared with the kriging models obtained from only using the DNS data (points ($\square$) in Figure 2) which we refer to as DNS GPR (Gaussian Process regression). A similar GP model that uses the RANS data (all ($\bigcirc$) points except ($\times$) in Figure 2) is referred to as RANS GPR. All the points except the samples ($\times$) in Figure 2 are used to train the linear multi-fidelity co-kriging model. The WSS occurring on the stenotic vessel is projected on the rectangle such that the length of the rectangle is the length of the stenotic vessel and the breadth is the range of azimuthal angle $[-\pi, \pi]$. Figure 5 shows the

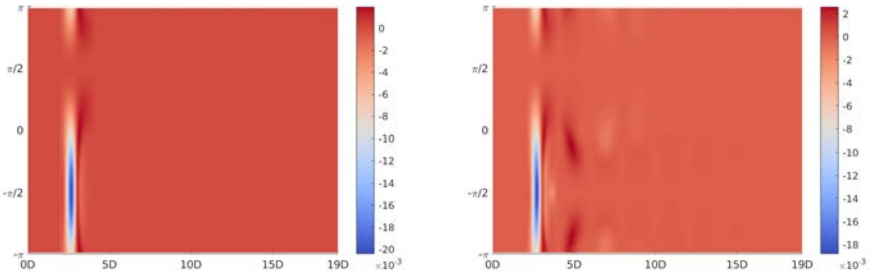

(a) DNS (b) RANS

Figure 5: The WSS contour for the DNS and RANS with (SI, E)=(40,100); the wall of the stenostic vessel is projected on to a rectangle with the length and breadth equal to the length of the vessel and the range of azimuthal angle respectively.

Table 1: $\pm 1.96\sigma$ around the predicted WSS along the streamwise direction for azimuthal angle 0 (refer to Figure 5) at the position of stenosis $2D$ to $4D$ using RANS GPR, DNS GPR, and co-kriging multi-fidelity model.

(SI,E)	RANS GPR	DNS GPR	Multi-fidelity model
(70,50)	2.005048	2.283755	0.133722
(60,30)	1.365022	1.623082	0.113875
(60,0)	0.903891	0.581707	0.120253
(50,80)	0.522102	0.698840	0.074726
(40,30)	2.425342	1.19060	0.144965

WSS contours for both DNS and RANS for the case, (SI, E)=(40,100) of the input variables (refer to Figure 2). The predictions for the five different (SI, E) are shown in Figure 6(a) - Figure 6(e) respectively. It can be inferred that the multi-fidelity co-kriging model predicts the WSS along a streamwise direction better than using the RANS GPR and DNS GPR in all the cases. Also, it can be seen that the kriging from the high-fidelity model (DNS GPR), by using the same points as in the multi-fidelity co-kriging model, obtains better predictions than the low-fidelity model (RANS GPR). The minimum value of the WSS in the stenotic zone is underestimated by RANS as seen from Figure 6(a) - Figure 6(e), also at certain instances leads to overshooting. The position of the minimum wall shear stress occurrence is also best estimated using the multi-fidelity model compared to the kriging models. The predictions and $\pm 1.96\sigma$ around the mean value of the predicted WSS is shown in the Table 1.

4 CONCLUSIONS

The current work aimed to obtain high-fidelity predictions of the quantities of interest in the space of the parameters by combining low-fidelity RANS and high-fidelity DNS. A straight blood vessel with the stenosis is studied with varying area reduction and eccentricity. The focus was to predict the WSS and mean pressure drop in the streamwise direction that occurred due to this in the stenotic region. An efficient method based on co-kriging that uses a difference factor between the two fidelity models and the correlation factor combines the low-fidelity data with high-fidelity data. This methodology can be applied to more complex cases with patient-specific geometries. Regarding computational performance, the method can be improved by studying the sensitivity within the parameter fields. The non-linear relationship between the data available from the different fidelities will be explored as an extension of the present work.

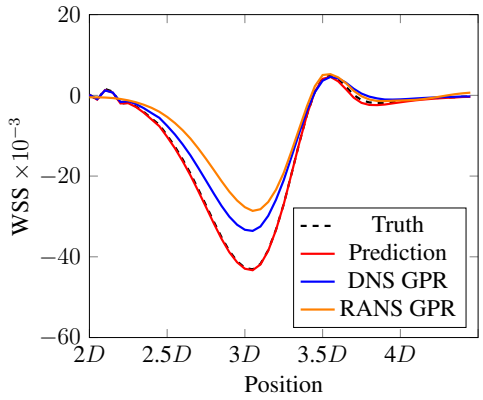

(a) (SI, E)=(70,50)

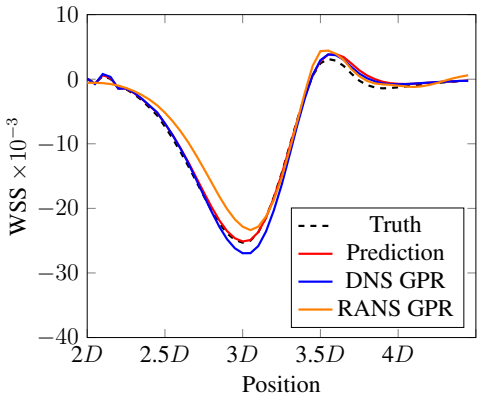

(b) (SI, E)=(60,30)

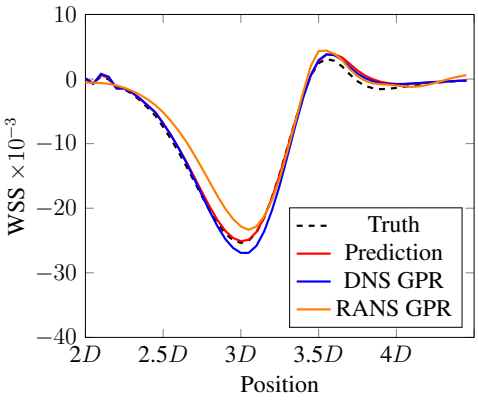

(c) (SI, E)=(60,0)

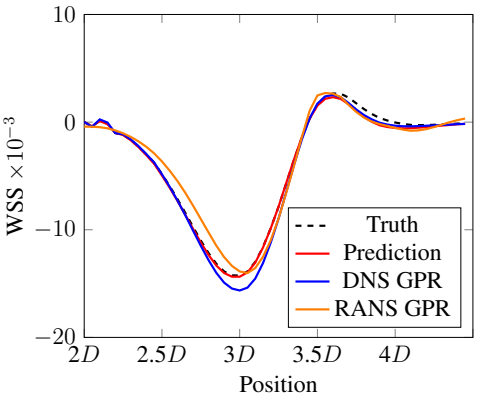

(d) (SI, E)=(50,80)

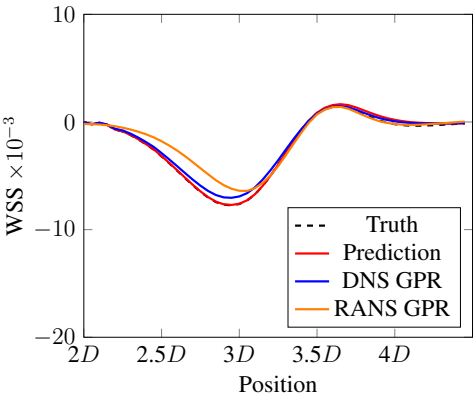

(e) (SI, E)=(40,30)

Figure 6: The prediction of the time-averaged WSS along the streamwise direction for azimuthal angle 0 (refer to Figure 5) at the position of stenosis $2D$ to $4D$, refer to Figure 1.

ACKNOWLEDGEMENTS

We acknowledge the financial support from the Department of Engineering Mechanics at KTH (Royal Institute of Technology) to the first author. The computations were enabled by resources in project SNIC 2022/3-25 provided by the National Academic Infrastructure for Supercomputing in Sweden (NAISS), funded by the Swedish Research Council through grant agreement no. 2022-06725.

REFERENCES

[1] V. Mancini, A. W. Bergersen, J. Vierendeels, P. Segers, and K. Valen-Sendstad, "High-frequency fluctuations in post-stenotic patient-specific carotid stenosis fluid dynamics: A computational fluid dynamics strategy study," *Cardiovascular Engineering and Technology*, vol. 10, pp. 277–298, 2019.

[2] A. Mahalingam, U. U. Gawandalkar, G. Kini, A. Buradi, T. Araki, N. Ikeda, A. Nicolaides, J. R. Laird, L. Saba, and J. S. Suri, "Numerical analysis of the effect of turbulence transition on the hemodynamic parameters in human coronary arteries," *Cardiovascular Diagnosis and Therapy*, vol. 6, no. 3, p. 208, 2016.

[3] A. Arnold, C. Battista, D. Bia, Y. Z. German, R. L. Armentano, H. Tran, and M. S. Olufsen, "Uncertainty quantification in a patient-specific one-dimensional arterial network model: Enkf-based inflow estimator," *Journal of Verification, Validation and Uncertainty Quantification*, vol. 2, no. 1, 2017.

[4] S. Khodaei, L. Garber, J. Bauer, A. Emadi, and Z. Keshavarz-Motamed, "Long-term prognostic impact of paravalvular leakage on coronary artery disease requires patient-specific quantification of hemodynamics," *Scientific Reports*, vol. 12, no. 1, p. 21357, 2022.

[5] C. Huang, B. Radi, and A. E. Hami, "Uncertainty analysis of deep drawing using surrogate model based probabilistic method," *The International Journal of Advanced Manufacturing Technology*, vol. 86, no. 9-12, pp. 3229–3240, 2016.

[6] R. B. Gramacy, *Surrogates: Gaussian process modeling, design, and optimization for the applied sciences*. CRC press, 2020.

[7] C. Lataniotis, S. Marelli, and B. Sudret, "Extending classical surrogate modeling to high dimensions through supervised dimensionality reduction: a data-driven approach," *International Journal for Uncertainty Quantification*, vol. 10, no. 1, 2020.

[8] C. E. Rasmussen and C. K. Williams, *Gaussian Processes for Machine Learning*, vol. 1. Springer, 2006.

[9] G. Matheron, "Principles of geostatistics," *Economic Geology*, vol. 58, no. 8, pp. 1246–1266, 1963.

[10] T. Østergård, R. L. Jensen, and S. E. Maagaard, "A comparison of six metamodeling techniques applied to building performance simulations," *Applied Energy*, vol. 211, pp. 89–103, 2018.

[11] J. R. Carr, D. E. Myers, and C. E. Glass, "Cokriging—a computer program," *Computers & Geosciences*, vol. 11, no. 2, pp. 111–127, 1985.

[12] M. C. Kennedy, C. W. Anderson, S. Conti, and A. O'Hagan, "Case studies in gaussian process modelling of computer codes," *Reliability Engineering & System Safety*, vol. 91, no. 10-11, pp. 1301–1309, 2006.

[13] P. Perdikaris, D. Venturi, and G. E. Karniadakis, "Multifidelity information fusion algorithms for high-dimensional systems and massive data sets," *SIAM Journal on Scientific Computing*, vol. 38, no. 4, pp. B521–B538, 2016.

[14] L. Le Gratiet and J. Garnier, "Recursive co-kriging model for design of computer experiments with multiple levels of fidelity," *International Journal for Uncertainty Quantification*, vol. 4, no. 5, 2014.

[15] J. Goh, D. Bingham, J. P. Holloway, M. J. Grosskopf, C. C. Kuranz, and E. Rutter, "Prediction and computer model calibration using outputs from multifidelity simulators," *Technometrics*, vol. 55, no. 4, pp. 501–512, 2013.

[16] S. Rezaeiravesh, T. Mukha, and P. Schlatter, "Efficient prediction of turbulent flow quantities using a Bayesian hierarchical multifidelity model," *arXiv preprint arXiv:2210.14790*, 2022.

[17] X. Meng, H. Babaee, and G. E. Karniadakis, "Multi-fidelity Bayesian neural networks: Algorithms and applications," *Journal of Computational Physics*, vol. 438, p. 110361, 2021.

[18] J. I. Madsen and M. Langthjem, "Multifidelity response surface approximations for the optimum design of diffuser flows," *Optimization and Engineering*, vol. 2, pp. 453–468, 2001.

[19] F. S. Costabal, P. Perdikaris, E. Kuhl, and D. E. Hurtado, "Multi-fidelity classification using gaussian processes: accelerating the prediction of large-scale computational models," *Computer Methods in Applied Mechanics and Engineering*, vol. 357, p. 112602, 2019.

[20] P. Perdikaris and G. E. Karniadakis, "Model inversion via multi-fidelity bayesian optimization: a new paradigm for parameter estimation in haemodynamics, and beyond," *Journal of The Royal Society Interface*, vol. 13, no. 118, p. 20151107, 2016.

[21] C. M. Fleeter, G. Geraci, D. E. Schiavazzi, A. M. Kahn, and A. L. Marsden, "Multilevel and multifidelity uncertainty quantification for cardiovascular hemodynamics," *Computer Methods in Applied Mechanics and Engineering*, vol. 365, p. 113030, 2020.

[22] R. Molléro, X. Pennec, H. Delingette, A. Garny, N. Ayache, and M. Sermesant, "Multifidelity-CMA: a multifidelity approach for efficient personalisation of 3d cardiac electromechanical models," *Biomechanics and modeling in mechanobiology*, vol. 17, pp. 285–300, 2018.

[23] H. Gao, X. Zhu, and J.-X. Wang, "A bi-fidelity surrogate modeling approach for uncertainty propagation in three-dimensional hemodynamic simulations," *Computer Methods in Applied Mechanics and Engineering*, vol. 366, p. 113047, 2020.

[24] K. Hoque, M. Ferdows, S. Sawall, E. Tzirtzilakis, and M. Xenos, "Hemodynamic characteristics expose the atherosclerotic severity in coronary main arteries: One-dimensional and three-dimensional approaches," *Physics of Fluids*, vol. 33, no. 12, p. 121907, 2021.

[25] A. Stein and L. Corsten, "Universal kriging and cokriging as a regression procedure," *Biometrics*, pp. 575–587, 1991.

[26] X. Yang, X. Zhu, and J. Li, "When bifidelity meets cokriging: An efficient physics-informed multifidelity method," *SIAM Journal on Scientific Computing*, vol. 42, no. 1, pp. A220–A249, 2020.

[27] S. S. Varghese, S. H. Frankel, and P. F. Fischer, "Direct numerical simulation of stenotic flows. part 1. steady flow," *Journal of Fluid Mechanics*, vol. 582, pp. 253–280, 2007.

[28] C. Moreno and K. Bhaganagar, "Modeling of stenotic coronary artery and implications of plaque morphology on blood flow," *Modelling and Simulation in Engineering*, vol. 2013, pp. 14–14, 2013.

[29] F. Menter, "Zonal two equation k-u turbulence models for aerodynamic flows. aiaa paper july 1993; 93-2906," in *24th Fluid Dynamics Conference*.

[30] R. Tabe, F. Ghalichi, S. Hossainpour, and K. Ghasemzadeh, "Laminar-to-turbulence and relaminarization zones detection by simulation of low Reynolds number turbulent blood flow in large stenosed arteries," *Bio-medical Materials and Engineering*, vol. 27, no. 2-3, pp. 119–129, 2016.

[31] M. A. K. Miah, S. Hossain, and S. Salehin, "Effects of severity and dominance of viscous force on stenosis and aneurysm during pulsatile blood flow using computational modelling," 2021.

[32] T. C. Gasser, "Continuum mechanics," in *Vascular Biomechanics: Concepts, Models, and Applications*, pp. 91–165, Springer, 2021.